concentrations of active R in the plant. This conclusion is consistent with a model proposing that trichome initiation is governed by transcription factors such as R or TTG plus GL1, a myb homolog required for trichome initiation along with TTG (*23*), and that a trichome can exert a local inhibition that prevents later developing cells nearby from producing trichomes. When this inhibition is attenuated a few cells away, another trichome is initiated, which in turn produces a local inhibition. The data presented here are consistent with a model in which the cell fate decision to be or not to be a trichome hinges on a competition between positive regulators, such as R or TTG and GL1, and a local inhibition produced by a committed trichome cell. Alternatively, the local inhibition may work before the activation of R or TTG in the trichome determination pathway, inhibition that is bypassed by the ectopic expression of R.

Factors in addition to the expression patterns of GL1 or TTG dictate the regular pattern of trichome formation on the wild-type leaf surface. Hybridization in situ indicates that GL1 is expressed uniformly in the epidermis of leaf primordia before trichome initiation (*24*). Genetic mosaic analysis with GL1 indicates that it acts locally (over no more than a few cell diameters) rather than over a long distance and that it may be strictly cell autonomous (*25*). The *ttg* gene is probably expressed in all leaf epidermal cells before trichome initiation. This expression is suggested by the observation that anthocyanin production, which also requires TTG, can be seen in developing leaves before trichome initials are observed (*17*). In one described trichome spacing mutant, *Try* (*25*), trichomes occur in clusters. This mutant may be defective in the production of a repressor or in the signal transduction from the repressor to trichome initiation.

Although the full-length GR can activate transcription from a GR-responsive, element-containing promoter in tobacco protoplasts (*8*), no activation was seen in stably transformed *Arabidopsis* plants. The R-GR fusion described here may serve to stabilize the ligand binding domain of the GR. Fusion of the steroid binding domain of the GR to other developmental regulators, particularly transcription factors, can be a valuable research tool in plants and other multicellular organisms in which transformation can be used to probe developmental timing and the nature of positional information. There are many other steroid receptors that function in a manner similar to that of GR (*26*), and these may prove equally valuable as specific conditional regulators of plant development or gene expression.

## REFERENCES AND NOTES


1. M. Koorneef, Arabidopsis *Inf. Serv.* **18**, 45 (1981); ———, *ibid.* **27**, 1 (1990).
2. M. E. Galway *et al.*, *Dev. Biol.*, in press.
3. A. M. Lloyd, V. Walbot, R. W. Davis, *Science* **258**, 1773 (1992).
4. S. R. Ludwig, B. Bowen, L. Beach, S. R. Wessler, *ibid.* **247**, 449 (1990); B. A. Roth, S. A. Goff, T. M. Klein, M. E. Fromm, *Plant Cell* **3**, 317 (1991); S. A. Goff, K. C. Cone, V. L. Chandler, *Genes Dev.* **6**, 864 (1992).
5. S. R. Ludwig, L. F. Habera, S. L. Dellaporta, S. R. Wessler, *Proc. Natl. Acad. Sci. U.S.A.* **86**, 7092 (1989).
6. M. Schena and K. R. Yamamoto, *Science* **241**, 965 (1988).
7. S. K. Yoshinaga and K. R. Yamamoto, *Mol. Endocrinol.* **5**, 844 (1991).
8. M. Schena, A. M. Lloyd, R. W. Davis, *Proc. Natl. Acad. Sci. U.S.A.* **88**, 10421 (1991).
9. D. Picard, S. J. Salser, K. R. Yamamoto, *Cell* **54**, 1073 (1988).
10. M. Eilers, D. Picard, K. R. Yamamoto, J. M. Bishop, *Nature* **340**, 66 (1989); G. Superti-Furga, G. Bergers, D. Picard, M. Busslinger, *Proc. Natl. Acad. Sci. U.S.A.* **88**, 5114 (1991); T. J. Hope, X. Huang, D. McDonald, T. G. Parslow, *ibid.* **87**, 7787 (1990).
11. S. M. Hollenberg, P. F. Cheng, H. Weintraub, *Proc. Natl. Acad. Sci. U.S.A.* **90**, 8028 (1993).
12. R. Miesfeld *et al.*, *Cell* **46**, 389 (1986).
13. The R-GR fusion is described in Fig. 1. It was placed in the plant transformation vector pKYLX71 (*3*, *15*). Complete construction details will be supplied on request.
14. P. N. Benfey, L. Ren, N.-H. Chua, *EMBO J.* **8**, 2195 (1989).
15. C. L. Schardl *et al.*, *Gene* **61**, 1 (1987).
16. D. Valvekens, M. Van Montagu, M. Van Lijsebettens, *Proc. Natl. Acad. Sci. U.S.A.* **85**, 5536 (1988).
17. A. M. Lloyd, unpublished data.
18. F. Quattrocchio, J. F. Wing, H. T. C. Leppen, J. N. M. Mol, R. E. Koes, *Plant Cell* **5**, 1497 (1993).
19. M. H. Williams and P. B. Green, *Protoplasma* **147**, 77 (1988).
20. H. H. Samuels and G. M. Tomkins, *J. Mol. Biol.* **52**, 57 (1970).
21. L. I. Held, *Bioessays* **13**, 633 (1991); S. Campuzano and J. Modolell, *Trends Genet.* **8**, 202 (1992).
22. R. W. Korn, *Dev. Biol.* **88**, 115 (1981).
23. D. G. Oppenheimer, P. L. Herman, S. Sivakumaran, J. Esch, M. D. Marks, *Cell* **67**, 483 (1991).
24. J. C. Larkin, D. G. Oppenheimer, S. Pollock, M. D. Marks, *Plant Cell* **5**, 1739 (1993).
25. M. Hülskamp, S. Misera, G. Jürgens, *Cell* **76**, 555 (1994).
26. B. O'Malley, *Mol. Endocrinol.* **4**, 363 (1990); R. F. Power, O. M. Conneely, B. W. O'Malley, *Trends Pharmacol. Sci.* **13**, 318 (1992).
27. H. Drumm-Herrel and H. Mohr, *Photochem. Photobiol.* **33**, 391 (1981).


28. We thank Dawn Frame for preparation of replica leaf molds and casts; C. Schardl, A. Hunt, P. Godowski, S. Wessler, C. Koncz, and M. Koornneef for donations of plasmids and strains; and M. Campbell, K. Marrs, A. B. Lloyd, and P. Green for critical reading of the manuscript. Supported by National Institutes of Health grants GM 32422 (V.W.) and R37-H600198 (R.W.D.) and National Science Foundation grant DMB-910601 (R.W.D.).

13 June 1994; accepted 29 August 1994


# Vancomycin Resistance: Structure of D-Alanine:D-Alanine Ligase at 2.3 Å Resolution


Chang Fan, Paul C. Moews, Christopher T. Walsh, James R. Knox*



**The molecular structure of the D-alanine:D-alanine ligase of the *ddlB* gene of *Escherichia coli*, co-crystallized with an *S*,*R*-methylphosphinate and adenosine triphosphate, was determined by x-ray diffraction to a resolution of 2.3 angstroms. A catalytic mechanism for the ligation of two D-alanine substrates is proposed in which a helix dipole and a hydrogen-bonded triad of tyrosine, serine, and glutamic acid assist binding and deprotonation steps. From sequence comparison, it is proposed that a different triad exists in a recently discovered D-alanine:D-lactate ligase (VanA) present in vancomycin-resistant enterococci. A molecular mechanism for the altered specificity of VanA is suggested.**


The bacterial cell wall and the enzymes that synthesize it are targets of many antibacterial agents, such as D-cycloserine, β-lactams (penicillins and cephalosporins), and glycopeptides (vancomycins). The construction of wall peptidoglycan requires a cross-linking of peptidyl moieties on adjacent glycan strands by transpeptidation between an amine group on one strand and the penultimate D-alanine of a D-Ala–D-Ala terminus on an adjacent strand. The transpeptidase or transpeptidases that catalyze this step are the target of β-lactam antibiotics (*1*, *2*). Vancomycin-type antibiotics, on the other hand, bind not to an enzyme but directly to the D-Ala–D-Ala terminus and inhibit cross-linking by the transpeptidase (*3*). In the face of β-lactamase production (*4*) and transpeptidase mutation (*1*, *2*), an attractive enzymic target for drug design is the D-alanine:D-alanine ligase (DD ligase) that produces one of the components of peptidoglycan (*5*).

Two isoforms of DD ligase from the *ddlA* and *ddlB* genes in *Escherichia coli* have been studied (*6*). The proposed mechanism for dipeptide formation begins with attack of


C. Fan, P. C. Moews, J. R. Knox, Department of Molecular and Cell Biology, University of Connecticut, Storrs, CT 06269–3125, USA.
C. T. Walsh, Department of Biological Chemistry and Molecular Pharmacology, Harvard Medical School, Boston, MA 02115, USA.
*To whom correspondence should be addressed.

the first D-alanine on the γ-phosphate of adenosine triphosphate (ATP) to yield an acylphosphate, followed by attack of the amino group of the second D-alanine to produce tetrahedral adduct **1** that then eliminates phosphate to give the DD dipeptide. The phosphinate analog **2** of the tetrahedral adduct has been shown to be a remarkably potent inhibitor (*7*), producing phosphinophosphate **3**, which dissociates from the *ddlA* ligase so slowly (a time scale of days) that it causes time-dependent inactivation (*8*). From an x-ray analysis (Table 1) of the *ddlB* DD ligase (DdlB) in complex with **3** and adenosine diphosphate (ADP), we propose a catalytic mechanism for the synthesis of D-Ala–D-Ala and propose how another ligase (VanA) detected in the late 1980s can produce a D-Ala–D-Lactate depsipeptide (*9*), resulting in a strong resistance in Gram-positive enterococci to vancomycin, the backup antibiotic in cases of β-lactam resistance (*10*).

**Table 1.** Crystallographic data, phasing, and refinement (*29*). Abbreviations are defined as follows: $d_{min}$ is minimum Bragg spacing or $\lambda/2 \sin\theta$, where $\lambda$ is the x-ray wavelength and $\theta$ is half the diffraction angle. $R_{sym} = \Sigma|I_i - \bar{I}|/\Sigma I_i$, where $I_i$ is an individual intensity observation and $\bar{I}$ is the averaged intensity. $R_{iso} = \Sigma|I_{PH} - I_P|/\Sigma|I_{PH} + I_P|$, where $I_{PH}$ and $I_P$ are the derivative and native intensities, respectively. Phasing power = $\Sigma|F_H(calc)|/\Sigma|E|$, where $F_H$ is the structure factor of the heavy atoms and $E$ (lack of closure error) = $|F_{PH}(obs)| - |F_{PH}(calc)|$. PIP is di-μ-iodobis(ethylenediamine)-di-platinum (II) nitrate, DMA is dimercury acetate, TMM is tetrakis(acetoxymercuri)methane, and Pt(en)$Cl_2$ is Pt(ethylenediamine) dichloride.

| Data | $d_{min}$ (Å) | Measurements (number) | Reflections (number) | $I/\sigma(I)$ | Completeness (%) | $R_{sym}$ (%) | $R_{iso}$ (%) | Phasing power/ resolution (Å) |
|---|---|---|---|---|---|---|---|---|
| Native | 2.3 | 83,021 | 11,014 | 14.1 | 90 | 5.7 | — | — |
| $CH_3HgOH$ | 2.3 | 91,755 | 10,298 | 14.4 | 84 | 6.5 | 14.7 | 3.4/3.0 |
| PIP | 3.0 | 43,412 | 5,301 | 10.4 | 94 | 6.9 | 14.8 | 1.5/3.0 |
| DMA | 2.8 | 59,105 | 6,677 | 13.2 | 97 | 6.4 | 16.4 | 3.1/3.0 |
| TMM | 2.8 | 48,566 | 5,954 | 12.7 | 86 | 7.3 | 16.9 | 2.7/3.0 |
| Pt(en)$Cl_2$ | 2.9 | 27,419 | 5,593 | 7.5 | 90 | 8.1 | 11.5 | 1.6/5.0 |
| $K_3UO_2F_5$ | 2.8 | 66,578 | 6,471 | 12.3 | 94 | 9.1 | 8.1 | 1.2/5.2 |
| $KAu(CN)_2$ | 3.0 | 31,206 | 5,188 | 4.9 | 92 | 11.1 | 10.7 | 1.4/5.6 |

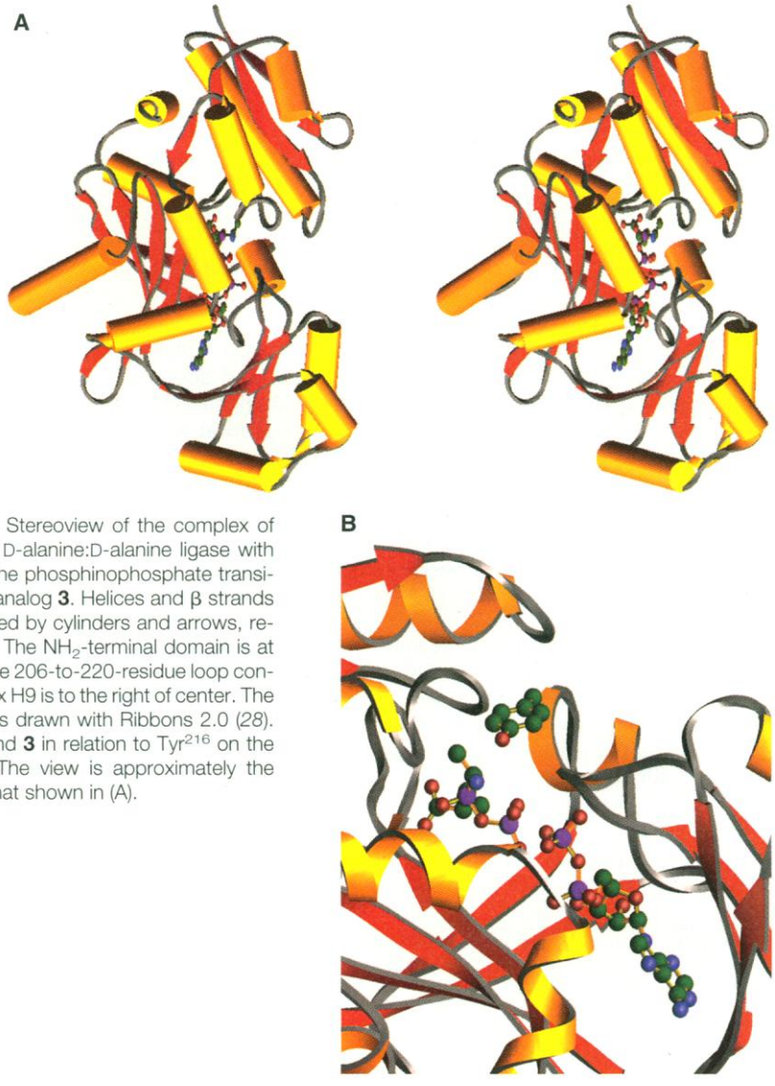


**Fig. 1.** (**A**) Stereoview of the complex of the *E. coli* D-alanine:D-alanine ligase with ADP and the phosphinophosphate transition-state analog **3**. Helices and β strands are indicated by cylinders and arrows, respectively. The $NH_2$-terminal domain is at the top. The 206-to-220-residue loop containing helix H9 is to the right of center. The picture was drawn with Ribbons 2.0 (*28*). (**B**) ADP and **3** in relation to $Tyr^{216}$ on the H9 helix. The view is approximately the same as that shown in (A).

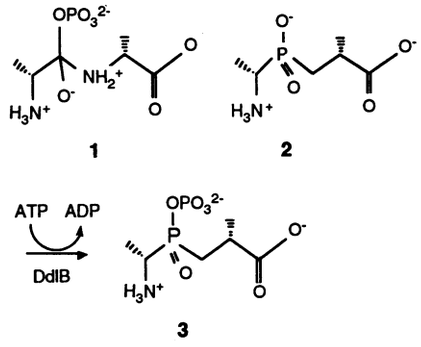


The tertiary structure of the complexed DD ligase is shown in Fig. 1. The molecule is dimeric across the crystallographic diad, with $Met^{75}$, $Leu^{78}$, $Val^{88}$, $Met^{89}$, $Ala^{92}$, $Leu^{93}$, $Leu^{102}$, and $Leu^{103}$ forming the interface. Secondary structure elements (Fig. 2) are clustered into $NH_2$-terminal, central, and COOH-terminal domains, each consisting of a β sheet of at least four strands. The $NH_2$-terminal β sheet differs from the other two sheets by having parallel β strands. Primarily, the central and COOH-terminal domains bind ATP or ADP. Surprisingly, the folding of DD ligase is found to be quite similar to that of *E. coli* glutathione synthetase (*11*), despite their low sequence homology. Two important peptide segments in the synthetase could not be mapped (*12*), segments that we believe correspond in DD ligase to the two loops described below.

ADP is sandwiched between two antiparallel β sheets, one each from the central and COOH-terminal domains. From an edge of the sandwich emanate two loops of residues 148 to 153 and 206 to 220 (Fig. 3). The first loop connects strands B6 and B7 and contains $Glu^{148}$-Gly-Ser-Ser-Val-Gly. Although this loop contains several glycines, like the so-called P loop of nucleotide-binding proteins (*13*), the glycines are not followed by the signature sequence Gly-Lys-Thr (Ser). The second loop between B10 and B11 contains short helix H9. The hydroxyl groups of $Ser^{150}$ and $Ser^{151}$ form three hydrogen bonds to H9 that hold the

loops over the catalytic cavity. A solvent accessibility calculation shows that only 2% of the surface area of ADP or **3** is exposed, demonstrating that the loops would be extremely effective in preventing solvent access to reactive intermediates.

In ADP the adenine base is oriented *anti* to the ribose sugar, and the chi angle relating them (O4′–C1′–N9–C8) is 40°. The pucker of the ribose ring is 3′ *endo*, and the conformation around the C4′–C5′ bond is *gauche*$^+$ (Fig. 4A). The adenine ring lies in a hydrophobic pocket formed by Ile$^{142}$, Met$^{159}$, and Phe$^{209}$ (Fig. 4B). The α and β phosphate groups form electrostatic links with Lys$^{97}$, Lys$^{144}$, and Lys$^{215}$ as well as a hydrogen bond with a main-chain NH of Ser$^{151}$. These and other interactions require the closing of the H9 loop (residues 206 to 220), thought to be flexible and exposed in the uncomplexed enzyme (*14*). We note that the invariant Lys$^{144}$ is within the sequence proposed (*6*) to be the ATP binding domain in other enzymes that bind acylphosphate intermediates.

The inhibitor 1(*S*)-aminoethyl [2-carboxy-2(*R*)-methyl-1-ethyl] phosphinic acid (**2**) is observed (Fig. 4A) as a phosphinophosphate **3** arising from phosphoryl transfer from ATP (*8*). Two $Mg^{2+}$ cations bridge between **3** and ADP. Electrostatic interaction of the inhibitor's α ammonium group with the carboxyl group of Glu$^{15}$ (at a distance of 2.8 Å) helps to orient the phosphinate (Fig. 4C). Its α-carboxylic acid group is held at the other end by hydrogen bonds to Ser$^{281}$ and to the NH of Leu$^{282}$. In the center, the terminal P–O bond accepts hydrogen bonds from an $NH_2$ group of Arg$^{255}$ and from the NH of Gly$^{276}$. We anticipate that the intermediate **1** would be oriented analogously during a catalytic cycle.

Determinants of inhibitor or substrate chirality are Val$^{18}$ and Leu$^{282}$, which contact the $NH_2$- and COOH-terminal D-center methyl groups, respectively. Little empty space exists around the $NH_2$-terminal methyl group, as expected from the high specificity for a methyl substituent at this position (*15*). A conserved His$^{63}$ is anchored by hydrogen bonds so that its ring plane is almost perpendicular to this D-methyl bond. There is more space around the COOH-terminal methyl group, in accord with the finding that other phosphinates having larger substituents at this D center (such as thiomethyl and *n*-heptyl) are also effective inhibitors (*7*). The proximity of the Tyr$^{216}$ hydroxyl group to the methylene group (3.5 Å) of **3** indicates a probable interaction with the COOH-terminal D-alanine substrate.

On the basis of the binding of the tetrahedral analog **3** and ADP observed here, we can propose a mechanism for the specificity and sequential participation of two D-alanine substrates, the first of which acts as an electrophilic partner and the second as a nucleophilic partner in the condensation. The first D-alanine is activated as the acylphosphate (Fig. 5). After the α-ammonium group of this ($NH_2$-terminal) D-alanine is positioned by Glu$^{15}$, the hydrogen bond interactions that are shown would anchor and polarize a C–O bond of the carboxylic acid group to set up the other carboxylate oxygen atom to attack the γ-phosphate of ATP. This phosphate transfer step is assisted by the $Mg^{2+}$ cations observed in the complex and yields D-alanyl acylphosphate, now activated for transfer to the α-amino group of the second D-alanine. The (COOH-terminal) D-alanine is oriented by the macrodipole moment of helix H11 and then hydrogen-bonded by Tyr$^{216}$, Ser$^{281}$, and Leu$^{282}$. The positioning of the phenolic OH of Tyr$^{216}$, in turn, is controlled by the hydrogen bond triad of Glu$^{15}$-Ser$^{150}$-Tyr$^{216}$ seen in the phosphinate complex. How deprotonation of the α-$NH_3^+$ group of this D-alanine ($pK_a \approx 10.5$) occurs is not clear, but it is facilitated by interaction with the triad and by the dipole field of helix H11. This process is the requisite step for the generation of the nucleophilic α-$NH_2$ form to attack the electrophilic carbonyl center of the D-alanyl acylphosphate. This reaction leads directly to intermediate **1**, where Arg$^{255}$ and the NH of Gly$^{276}$ would stabilize this high-energy species, in an analogy to the observed interaction with **3**. Decomposition of **1** with the loss of phosphate yields D-Ala–D-Ala. The antibiotic and known inhibitor of DD-ligase, D-cycloserine (*15*), can be shown by modeling to form similar interactions with this environment, especially in the $NH_2$-terminal D-alanine site.

One of the corollaries of the structure of the complex of DD-ligase with **3** is the insight it may provide into the molecular basis of clinical resistance to the vancomycin antibiotics (*16*–*18*). In Gram-positive bacteria that have developed vancomycin resistance, a set of five genes is necessary and sufficient to bring about this trait. One

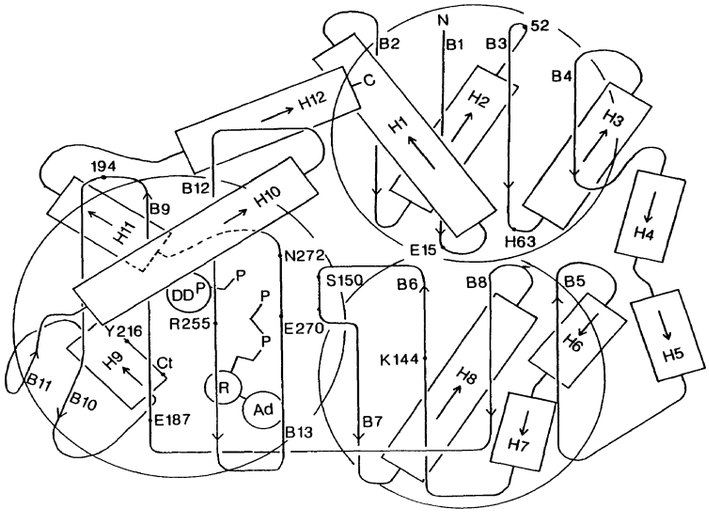


**Fig. 2.** Secondary structure for the three domains (circled) of DD ligase. Helices (H*n*) and β strands (B*n*) are indicated by rectangles and arrows, respectively. Structure assignments are as follows: residues 4 to 10 (B1), 16 to 32 (H1), 36 to 41 (B2), 48 to 52 (H2), 57 to 61 (B3), 71 to 79 (H3), 83 to 85 (B4), 88 to 95 (H4), 97 to 106 (H5), 113 to 117 (B5), 119 to 124 (H6), 128 to 137 (H7), 141 to 145 (B6), 154 to 158 (B7), 163 to 172 (H8), 176 to 181 (B8), 186 to 192 (B9), 197 to 206 (B10), 212 to 217 (H9), 221 to 225 (B11), 231 to 247 (H10), 253 to 260 (B12), 265 to 272 (B13), 282 to 289 (H11), 294 to 303 (H12). The abbreviations Ad, Rb, and P show the approximate locations of adenine, ribose, and phosphate groups, respectively, in the ADP and phosphinophosphate **3** (DD-P-P), and Ct is the cleavage position of the native enzyme by chymotrypsin. Points of insertion in the VanA ligase are predicted near 52 and 194. Helix H7 may be deleted in VanA.

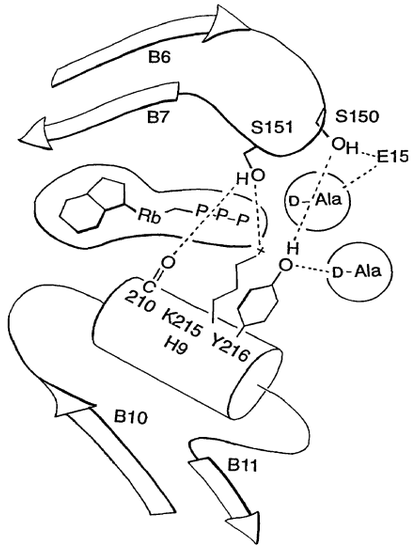


**Fig. 3.** Hydrogen bonds holding loops 148 to 153 and 206 to 220 over the nucleotide and substrate cavity. Differences thought to exist in VanA are K$^{215}$E and Y$^{216}$K (*20*).

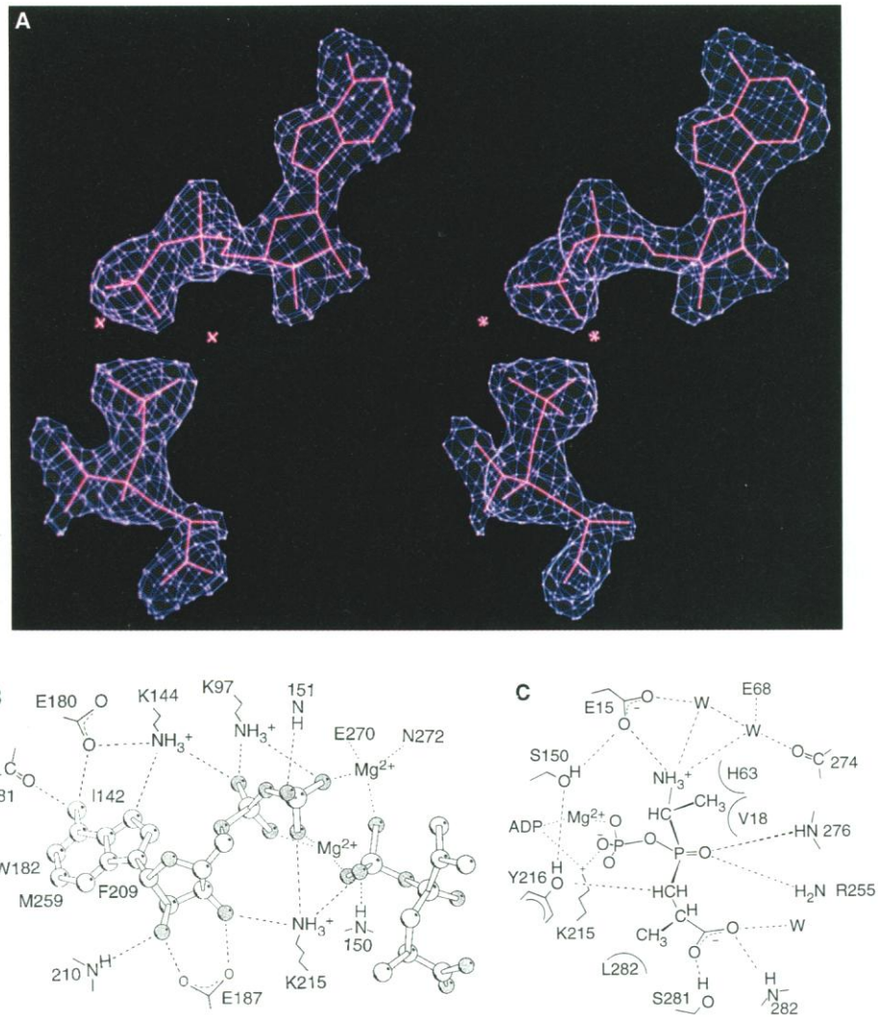


**Fig. 4.** (**A**) Difference electron density of ADP and phosphinophosphate **3**, bridged by two $Mg^{2+}$ cations. Coefficients are $|F_o| - |F_c|$ with both molecules excluded from the phasing. The contour level is 4σ. (**B**) Environment around the ADP molecule. Possible interactions are indicated by dashed lines. (**C**) Environment of the phosphorylated 1(*S*)-aminoethyl [2-carboxy-2(*R*)-methyl-1-ethyl] phosphinic acid **3**. Water molecules are indicated by W. Hydrogen bond distances in the triad $Y^{216}$ to $S^{150}$ and $S^{150}$ to $E^{15}$ are 2.8 and 2.6 Å, respectively.

**Fig. 5.** Proposed catalytic mechanism for the formation of D-Ala–D-Ala by DdlB DD ligase. Helix H11 is represented by the rectangle.

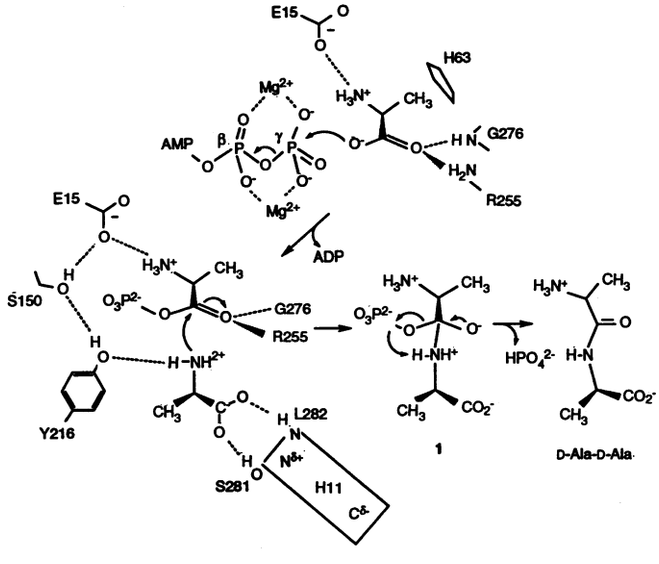


of those gene products, VanA, is a DdlB homolog that nevertheless shows altered specificity and functions as a depsipeptide ligase, making the ester D-Ala–D-lactate (*9*). The ester is able to serve as a transpeptidase substrate for the final cross-linking of the cell wall. The D-lactate ester has at least 1000-fold lessened binding affinity with vancomycin than has the normal acyl D-Ala–D-Ala (*3*, *9*, *18*).

The sequence of the enterococcal VanA ligase (*16*) has 28 to 32% identity, or about 45% similarity, with the DdlB DD ligase. Examination of their alignment in view of this crystal structure, as well as proteolysis and photoaffinity-labeling studies of DdlB (*14*), suggests that the tertiary structures of the two ligases are similar (*19*). The critical $Glu^{15}$, $Ser^{150}$, and $Ser^{281}$ are conserved, as are most residues shown in Fig. 4, B and C. Notable differences occur at DdlB positions 215 and 216 on the important H9 loop (*20*) near the bound inhibitor (Fig. 1B). The difference at 215, a radical change of Lys to Glu, may be compensated by a Leu-to-Arg change at position 282. An electrostatic linkage between 215 and the nearby 282 would anchor the H9 loop and contain the hydroxy acid substrate in the catalytic site. Functionally, a more significant change in the VanA catalytic site may be the substitution of Lys for $Tyr^{216}$. Given the role proposed in Fig. 5 for the phenolic OH of $Tyr^{216}$, the presence of the cationic Lys in VanA is intriguing. Even with differences at positions 215, 216, and 282, each ligase conserves a net positive charge near the phosphate groups of ATP and ADP, as well as a hydrogen bond between an ammonium group and an oxygen atom (Fig. 6). The direction of this interaction is simply reversed in the two enzymes.

Mechanistically, the $\epsilon$-$NH_3^+$ group of $Lys^{216}$ (DdlB numbering) in VanA could be the molecular gate that disfavors the binding of D-alanine by electrostatic repulsion toward its $\alpha$-$NH_3^+$ group and instead favors productive hydrogen bonding of the α-OH of D-lactate. The lysyl-$\epsilon$-$NH_3^+$ group could serve another role by assisting deprotonation of the less acidic α-OH group of D-lactate ($pK_a \approx 14$), a reaction apparently not attainable by the $Tyr^{216}$ conserved in

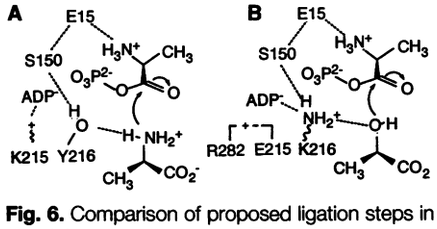


**Fig. 6.** Comparison of proposed ligation steps in (**A**) wild-type DD ligase and (**B**) VanA.

wild-type ligases. Thus, the change at position 216 may determine the activation energy and whether D-alanine or D-lactate is attached to D-alanyl acylphosphate, leading to D-Ala–D-Ala and ultimate vancomycin sensitivity or to D-Ala–D-lactate and vancomycin resistance.

To the extent that **1** would be oriented as is **3** in the active site, the role of several residues in catalysis and specificity are implicated and will be subsequently tested by mutagenesis. The structure-based design of novel inhibitors should now be possible for both wild-type DD ligases and modified ligases arising under the pressure of vancomycin usage (*10*, *18*).

## REFERENCES AND NOTES


1. J.-M. Frere, M. Nguyen-Disteche, J. Coyette, B. Joris, in *The Chemistry of β-Lactams*, M. I. Page, Ed. (Blackie Academic & Professional, London, 1992), pp. 148–197.
2. B. G. Spratt, *Science* **264**, 388 (1994).
3. G. D. Wright and C. T. Walsh, *Acct. Chem. Res.* **25**, 468 (1992).
4. S. G. Waley, in (*1*), pp. 198–228; J. Davies, *Science* **264**, 375 (1994).
5. F. C. Neuhaus, *J. Biol. Chem.* **237**, 778 (1962); and W. P. Hammes, *Pharmacol. Ther.* **14**, 265 (1981); C. T. Walsh, *J. Biol. Chem.* **264**, 2393 (1989).
6. L. E. Zawadzke, T. D. H. Bugg, C. T. Walsh, *Biochemistry* **30**, 1673 (1991).
7. W. H. Parsons *et al.*, *J. Med. Chem.* **31**, 1772 (1988).
8. A. E. McDermott *et al.*, *Biochemistry* **29**, 5767 (1990).
9. T. D. H. Bugg *et al.*, *ibid.* **30**, 10408 (1991).
10. H. C. Neu, *Science* **257**, 1064 (1992); J. Travis, *ibid.* **264**, 360 (1994).
11. C. T. Walsh and J. R. Knox, unpublished results.
12. H. Yamaguchi *et al.*, *J. Mol. Biol.* **229**, 1083 (1993); T. Tanaka *et al.*, *Biochemistry* **32**, 12398 (1993).
13. M. Saraste, P. R. Sibbald, A. Wittinghofer, *Trends Biochem. Sci.* **15**, 430 (1990).
14. G. D. Wright and C. T. Walsh, *Protein Sci.* **2**, 1765 (1993).
15. F. C. Neuhaus, *J. Biol. Chem.* **237**, 3128 (1962); _____ and J. L. Lynch, *Biochemistry* **3**, 471 (1964); J. L. Strominger, E. Ito, R. H. Threnn, *J. Am. Chem. Soc.* **82**, 998 (1960).
16. S. Dutka-Malen, C. Molinas, M. Arthur, P. Courvalin, *Mol. Gen. Genet.* **224**, 364 (1990).
17. M. Arthur and P. Courvalin, *Antimicrob. Agents Chemother.* **37**, 1563 (1993).
18. C. T. Walsh, *Science* **261**, 308 (1993).
19. The folded structures may differ at three points (see Fig. 2): (i) A 43-residue segment of VanA is inserted near position 52 between helix H2 and strand B3; (ii) an eight-residue insertion exists near 194 between B9 and B10; and (iii) an eight-residue deletion results in the loss of surface helix H7. The first two insertions may appear in VanA as surface segments between rigid secondary structures.
20. Our alignment of the sequences containing the H9 loop, which differs slightly from other alignments (*16*, *21*), is

| | |
|---|---|
| DdlA | YAYDTKYIDED |
| DdlB | YDYEAKYLSDE (220) |
| VanA | QEVEPEKGSEN |
| VanC | FDFEEKYQLIS |

(Single-letter abbreviations for the amino acid residues are as follows: A, Ala; C, Cys; D, Asp; E, Glu; F, Phe; G, Gly; H, His; I, Ile; K, Lys; L, Leu; M, Met; N, Asn; P, Pro; Q, Gln; R, Arg; S, Ser; T, Thr; V, Val; W, Trp; and Y, Tyr.) While the EKY sequence of VanC could match either the EK of VanA or the KY of DdlA and DdlB, other matches favor the latter. Further, the existence of KY in VanC is compatible with our mechanism for peptide synthesis in DdlB, because the VanC ligase produces a peptide, D-Ala–D-Ser, rather than a depsipeptide (*21*).
21. S. Dutka-Malen, C. Molinas, M. Arthur, P. Courvalin, *Gene* **112**, 53 (1992); P. E. Reynolds, H. A. Snaith, A. J. Maguire, S. Dutka-Malen, P. Courvalin, *Biochem. J.* **301**, 5 (1994).
22. A. J. Howard *et al.*, *J. Appl. Crystallogr.* **20**, 383 (1987).
23. W. Furey and S. Swaminathan, *Am. Crystallogr. Assoc. Abstr.* **18**, 73 (1990).
24. J. S. Jack, *J. Mol. Graphics* **6**, 224 (1988).
25. T. A. Jones, *Methods Enzymol.* **115**, 157 (1985).
26. A. T. Brünger, *X-PLOR Manual, Version 2.1* (Yale University, New Haven, CT, 1990).
27. J. H. Konnert and W. A. Hendrickson, *Acta Crystallogr. Sect. A* **36**, 344 (1980).
28. M. Carson, *J. Mol. Graphics* **5**, 103 (1987).
29. The DD-ligase, purified as described (*6*), was co-crystallized with ATP and **2** by the hanging drop method. The drop contained enzyme (10 mg/ml) in the presence of 5 mM ATP and 5 mM **2** in 20% (v/v) ammonium sulfate at pH 7.0 in Hepes buffer with 1 mM $MgCl_2$ and $NaN_3$. The drop was suspended over 45% (v/v) ammonium sulfate at pH 5.5 in MES buffer. Crystals up to 0.6 by 0.4 mm grew over a few weeks in space group $P2_12_12$, with one molecule in the asymmetric unit. Cell dimensions are $a$ = 99.32 Å, $b$ = 51.44 Å, and $c$ = 51.22 Å. Diffraction data were collected on a Siemens area x-ray detector with a Rigaku rotating anode x-ray generator operating at 38 kV and 180 mA with graphite-monochromatized Cu-Kα radiation. Data reduction was done with the program XENGEN (*22*). Phases were obtained by the method of multiple isomorphous replacement with anomalous scattering by use of the program PHASIT (*23*). With seven derivatives contributing to 3.0 Å resolution, the mean figure-of-merit for 5512 reflections with $F > 0$ was 0.86. Fitting of the map with all 306 residues was done with CHAIN (*24*) and FRODO (*25*). The $R$ factor for a starting model, exclusive of ADP and **3**, was 0.43 to 3 Å resolution. When an initial refinement with X-PLOR (*26*) reached $R$ = 0.24 for 9501 reflections [$F > 3\sigma(F)$] from 10.0 to 2.3 Å resolution, ADP and **3** were fitted into a $2F_o - F_c$ map. Continued refinement with PROLSQ (*27*) with the addition of 292 water molecules produced a final $R$ factor of 0.172 for 9776 $3\sigma(F)$ data from 15.0 to 2.3 Å. Root-mean-square deviations of bonds and angles from ideal values are 0.013 Å and 1.7°, respectively. Coordinates have been deposited in the Protein Data Bank at the Brookhaven National Laboratory, Upton, NY (entry 1DLN).


30. We thank T. D. H. Bugg and G. D. Wright for supplying purified DD-ligase, P. A. Bartlett for generously providing the phosphinate **2**, and E. Lobkovsky and Y. Shi for helpful discussions. Supported by National Institutes of Health grants 1RO1-AI-34330 (J.R.K.) and GM-49338 (C.T.W.).

2 June 1994; accepted 6 September 1994


# c-Fos: A Key Regulator of Osteoclast-Macrophage Lineage Determination and Bone Remodeling


Agamemnon E. Grigoriadis, Zhao-Qi Wang, Marco G. Cecchini, Willy Hofstetter, Rolf Felix, Herbert A. Fleisch, Erwin F. Wagner*



**Mice lacking the proto-oncogene c-*fos* develop the bone disease osteopetrosis. Fos mutant mice were found to have a block in the differentiation of bone-resorbing osteoclasts that was intrinsic to hematopoietic cells. Bone marrow transplantation rescued the osteopetrosis, and ectopic c-*fos* expression overcame this differentiation block. The lack of Fos also caused a lineage shift between osteoclasts and macrophages that resulted in increased numbers of bone marrow macrophages. These results identify Fos as a key regulator of osteoclast-macrophage lineage determination in vivo and provide insights into the molecular mechanisms underlying metabolic bone diseases.**


The c-Fos oncoprotein is a component of the AP-1 transcription factor complex and is a member of a multigene family, including the *fos*-related (*fosB*, *fra-1*, *fra-2*) and *jun*-related (c-*jun*, *junB*, *junD*) genes (*1*). The function of Fos is dependent on formation of heterodimers with specific Jun proteins, but also with other leucine zipper–containing molecules, and subsequent binding to specific regulatory sequences (*1*). Because different dimer combinations can confer AP-1–dependent gene transcription in different cell types, it is a challenge to identify the biological processes in which the individual AP-1 family members are essential molecules, as opposed to those in which specific gene function may be redundant.

Overexpression of c-*fos* in transgenic and chimeric mice causes osteosarcomas and chondrosarcomas through mechanisms that involve specific transformation of osteogenic and chondrogenic cells, respectively (*2*, *3*). Mice lacking Fos develop osteopetrosis as a primary pathology and also exhibit altered hematopoiesis (*4*). The hematopoietic defects are secondary to the altered bone environment, because Fos mutant hematopoietic stem cells are capable of reconstituting lethally irradiated wild-type mice (*5*). However, the causal role of Fos in osteopetrosis is not yet known.

Mammalian osteopetroses are disorders of bone metabolism characterized by a reduction in osteoclast function, resulting in a net increase in skeletal mass (*6*). Bone remodeling is a dynamic process whereby osteoclastic bone resorption is tightly coupled to osteoblastic bone formation (*7*, *8*).


A. E. Grigoriadis, Z.-Q. Wang, E. F. Wagner, Research Institute of Molecular Pathology (IMP), Dr. Bohr-Gasse 7, A-1030 Vienna, Austria.
M. G. Cecchini, W. Hofstetter, R. Felix, H. A. Fleisch, Department of Pathophysiology, University of Berne, Murtenstrasse 35, CH-3010 Berne, Switzerland.
*To whom correspondence should be addressed.